Am J Physiol Renal Physiol 286: F170–F179, 2004.
First published September 9, 2003; 10.1152/ajprenal.00223.2003.

Application of difference gel electrophoresis to the identification of inner medullary collecting duct proteins

Jason D. Hoffert, Bas W. M. van Balkom, Chung-Lin Chou, and Mark A. Knepper
Laboratory of Kidney and Electrolyte Metabolism, National Heart, Lung, and Blood Institute, National Institutes of Health, Bethesda, Maryland 20892

Submitted 13 June 2003; accepted in final form 2 September 2003

Hoffert, Jason D., Bas W. M. van Balkom, Chung-Lin Chou, and Mark A. Knepper. Application of difference gel electrophoresis to the identification of inner medullary collecting duct proteins. *Am J Physiol Renal Physiol* 286: F170–F179, 2004. First published September 9, 2003; 10.1152/ajprenal.00223.2003.—In this study, we present a standardized approach to purification of native inner medullary collecting duct (IMCD) cells from rat kidney for proteomic analysis and apply the approach to identification of abundant proteins utilizing two-dimensional difference gel electrophoresis (DIGE) coupled with matrix-assisted laser desorption-ionization-time of flight mass spectrometry. Fractionation of inner medullary cell suspensions by low-speed centrifugation gave a highly purified IMCD cell fraction in which aquaporin-2 was enriched 10-fold. When DIGE was initially applied to rat inner medullas fractionated into IMCD cells (labeled with Cy3) and non-IMCD cells (labeled with Cy5), we identified 50 highly abundant proteins expressed in the IMCD cells. These proteins, identifiable without subcellular fractionation, included chiefly enzymes, structural proteins, and signaling intermediates. An additional 35 proteins were found predominantly in the non-IMCD cell types. Proteins that were highly enriched in the IMCD fraction included cytokeratin 8, cytokeratin 18, transglutaminase II, aminopeptidase B, T-plastin, heat shock protein (HSP) 27, HSP70, and lactate dehydrogenase A. Semiquantitative immunoblotting and immunohistochemistry confirmed relative expression levels and distribution of selected proteins. An additional 40 IMCD proteins were identified in separate experiments aimed at further enrichment of proteins through optimization of sample loading. These studies document the applicability of a standardized approach to purification of IMCD cells for proteomic analysis of IMCD proteins and demonstrate the feasibility of large-scale identification of proteins in the native IMCD cell.

inner medullary collecting duct; kidney; two-dimensional electrophoresis; difference gel electrophoresis; proteomics

THE COLLECTING DUCT, THE TERMINAL portion of the mammalian renal tubule, plays an important role in the regulation of water and salt balance (14). As is the case for other renal tubule segments, the collecting duct is highly specialized in both structure and function, expressing a subset of membrane channels including α-, β-, and γ-epithelial Na^+ channel (ENaC; see Ref. 7) and aquaporins (AQP)-2, -3, and -4 (25), which play central roles in regulation of Na^+ and water excretion in response to vasopressin, aldosterone, and other mediators. The collecting duct system itself is varied in properties, and the inner medullary collecting duct (IMCD) part differs in many respects with cortical and outer medullary parts. Traditionally, studies of the IMCD have focused on specific physiological processes or individual proteins. This "reductionist" method has been highly successful in broadening our understanding of IMCD function, but our knowledge is far from complete. The overall function of the IMCD cell undoubtedly depends on a large network of proteins. Recently, new methods for large-scale identification of proteins, i.e., proteomics, have been developed. Proteomics is broadly defined as "the systematic analysis of proteins for their identity, quantity, and function" (26). These methods can potentially fulfill the first step toward development of comprehensive systems models of individual cell types by identifying the "roster" of proteins expressed in such cells. Such "discovery" approaches have the potential of identifying novel hypotheses that can guide further experimentation.

Here we describe and characterize an approach to large-scale purification of native IMCD cells for proteomic analysis and then use a relatively new proteomic technique called difference gel electrophoresis (DIGE; see Ref. 31) to identify abundant IMCD proteins identifiable on 2-dimensional (2-D) gels without subcellular fractionation. DIGE is based on covalent labeling of proteins with either Cy3 or Cy5 fluorescent dyes, which improves the sensitivity and dynamic range of protein detection in 2-D gels. When two populations of proteins are to be compared, they can be labeled with different dyes and run on the same 2-D gel, allowing facile quantitative comparison of the relative abundances of individual proteins by analyzing separate Cy3 and Cy5 images. This virtually eliminates gel-gel variation as a factor in the analysis and decreases the time required for spot detection and quantitation. [See a recent review paper by Knepper (15) for a more thorough description of the technique.] This system has recently been used in an analysis of the mitochondrial proteome from mouse heart (12), in a study of the *Escherichia coli* proteome after benzoic acid treatment (33), and in a study of laser capture-microdissected esophageal carcinomas (35).

In this paper, we have applied the 2-D DIGE technique to the identification of IMCD proteins. The general approach was to carry out cell fractionation from inner medullas of rat kidneys and then to use DIGE to compare IMCD and non-IMCD cell fractions. The latter contains predominantly a mixture of structures including loops of Henle, vasa recta, and interstitial cells. The objective of this paper was to describe and characterize an approach to large-scale purification of native IMCD cells from rats and demonstrate the feasibility of large-scale identification of abundant proteins in a single renal cell type, the IMCD cell, i.e., those proteins that can be detected as spots using the DIGE technique without subcellular fractionation.

METHODS

Animals. Pathogen-free male Sprague-Dawley rats (National Cancer Institute-Frederick Cancer Research Facility, Frederick, MD) were

Address for reprint requests and other correspondence: M. A. Knepper, National Institutes of Health, Bldg. 10, Rm. 6N260, 10 Center Dr. MSC 1603, Bethedsa, MD 20892-1603 (E-mail: knep@helix.nih.gov).

The costs of publication of this article were defrayed in part by the payment of page charges. The article must therefore be hereby marked "*advertisement*" in accordance with 18 U.S.C. Section 1734 solely to indicate this fact.

maintained on an autoclaved pelleted rodent chow (413110–75–56; Zeigler Brothers, Gardners, PA) and ad libitum drinking water. All experiments were conducted in accord with an animal protocol approved by the Animal Care and Use Committee of the National Heart, Lung, and Blood Institute (Animal Care and Use Committee protocol number 2-KE-3).

Materials. *N*-hydroxy succinimide ester Cy3 and Cy5 dyes, as well as all reagents for running 2-D electrophoresis, were purchased from Amersham Biosciences (Piscataway, NJ). Sypro Ruby gel stain was from Molecular Probes (Eugene, OR). The bicinchoninic acid (BCA) protein assay kit was from Pierce (Rockford, IL). Urea transporter-B (UT-B) rabbit polyclonal antibody was kindly provided by Dr. Jeff M. Sands, Emory University (Atlanta, GA; see Ref. 30). AQP2 antibody (cc256) is an affinity-purified chicken polyclonal antibody raised against the carboxy-terminus of rat AQP2, SVELHSPQSLPRGSKA. A guinea pig polyclonal antibody that recognizes both cytokeratin 8 and cytokeratin 18 from rat was purchased from Research Diagnostics (Flanders, NJ). Transglutaminase type II goat polyclonal antibody was from Upstate Biotechnology (Lake Placid, NY). All other antibodies were from Santa Cruz Biotechnology (Santa Cruz, CA).

Preparation of IMCD and non-IMCD suspensions. IMCD and non-IMCD suspensions were prepared from inner medulla of rat kidney using the method of Stokes et al. (29) with a few modifications (2). Rats weighing 150–200 g were killed by decapitation, the kidneys were removed, and inner medullas were dissected and finely minced with a razor blade. The minced tissue was transferred to a 12 × 75-mm glass tube containing dissection fluid (118 mM NaCl, 25 mM $NaHCO_3$, 5 mM KCl, 4 mM Na_2HPO_4, 1.2 mM $MgSO_4$, 2 mM $CaCl_2$, and 5.5 mM glucose equilibrated with 95% air-5% CO_2 for 20 min) containing 2 mg/ml collagenase B (Boeringer Mannheim, Indianapolis, IN) and 600 U/ml hyaluronidase (Worthington Biochemical, Freehold, NJ). The sample was incubated at 37°C in this solution for 60–90 min with CO_2 equilibration. The suspension was aspirated with a large-bore Pasteur pipette every 15 min to break up large tissue fragments. After incubation, the sample was centrifuged at 80 *g* for 30 s to enrich for heavier IMCD structures, followed by centrifugation of the supernatant at 1,500 *g* for 5 min to pellet lighter non-IMCD fragments. Pellets were washed with dissection fluid and resuspended in either tissue homogenization buffer for immunoblotting or lysis buffer for 2-D electrophoresis.

Sample preparation and 2-D electrophoresis. Tissue suspensions were solubilized in lysis buffer containing 7 M urea, 2 M thiourea, 4% 3-[(3-cholamidopropyl)dimethylammonio]-1-propanesulfonate (CHAPS), and 30 mM Tris, pH 8.8. Lysates were then passed through a 21-gauge needle to shear the DNA and then centrifuged at 14,000 *g* for 15 min to pellet any insoluble material. Protein concentration of the cleared samples was determined using the 2-D Quant kit (Amersham). Pooled IMCD and non-IMCD samples from three rats were minimally labeled with Cy3 and Cy5 dyes, respectively, giving a final dye-to-protein ratio ≤1. Protein (50 μg) was labeled with 400 pmol Cy3 or Cy5 fluorescent dye, and the reaction was quenched by adding 10 mM lysine. Cy3- and Cy5-labeled samples were mixed together, and rehydration buffer was added (7 M urea, 2 M thiourea, 4% CHAPS, 0.5% pharmalytes, 40 mM DTT, and 0.002% bromphenol blue). The mixed sample was then loaded on a single precast immobilized pH gradient strip (24 cm; pH 3–10) for isoelectric focusing (IPGphor apparatus; Amersham) according to the following protocol: 30 V for 12 h (active rehydration), 500 V for 500 Vh, 1,000 V for 1,000 Vh, and 8,000 V for 62,500 Vh. After being focused, strips were equilibrated for 15 min in a solution containing 6 M urea, 30% glycerol, 2% SDS, 50 mM Tris·HCl, pH 8.8, 0.002% bromphenol blue, and 10 mg/ml DTT followed by a second 15-min equilibration with iodoacetamide (25 mg/ml) instead of DTT. Strips were briefly rinsed in 1× SDS-PAGE buffer and applied to a 12.5% polyacrylamide gel for electrophoresis at a constant 1–2 W/gel overnight.

Image analysis, spot picking, and mass spectrometry. Cy3 and Cy5 images were collected using a Typhoon scanner in fluorescence mode (Amersham). Final images were scanned at a resolution of 100 μm. Gels were fixed in 30% ethanol and 7.5% acetic acid for 2 h followed by Sypro Ruby staining overnight for total protein visualization. Statistics, quantitation, and gel matching were carried out on DeCyder software (Amersham). Spots of interest were matched to the Sypro-stained image before picking. This step is important for accurate spot picking, since attached Cy dye fluors (500 Da) can have a small but significant effect on the mass of low-molecular-weight proteins.

Spots of interest were processed by the fully automated Spot Handling Workstation (Amersham). Briefly, gel plugs were washed with 50 mM ammonium bicarbonate-50% methanol followed by 50% acetonitrile-0.1% trifluoroacetic acid (TFA) and then 90% acetonitrile for drying. After trypsin digestion in 20 mM ammonium bicarbonate, extracted peptides were dried and resuspended in 50% acetonitrile-0.5% TFA and mixed with α-cyano-4-hydroxycinnamic acid matrix on a matrix-assisted laser desorption ionization- (MALDI) target slide.

Peptide extracts were analyzed on a MALDI-time of flight (TOF) pro mass spectrometer operating in positive ion reflectron mode at 20 kV accelerating potential with eight-shot pulsed extraction enabled. Trypsin autodigestion peaks were used as internal calibrants. Peptide masses were searched against the National Center for Biotechnology Information nonredundant rat database using a proprietary implementation of ProFound, a program that calculates the likelihood of the correct identification based on the theoretical number of peptides in a trypsin digest of a given protein and the number of peptides matched (34). With this program, Bayes' probability theory and the maximum entropy principle are applied to derive the probability (*P*) for a correct identification. In this paper, we report the expectation value, which is essentially $1 - P$. Alkylation of all cysteines and oxidation of some methionines were assumed. An identification was considered accurate if the expectation value was below 0.1 (<10% chance of error) and the position of the spot on the 2-D gel approximately reflected the theoretical isoelectric point (pI) and molecular weight of the specified protein. Selected identifications were confirmed by immunoblotting of isolated IMCD cells from separately prepared rats that underwent the identical treatment protocol.

Immunoblotting. Tissue samples were homogenized in isolation buffer (10 mM triethanolamine, 250 mM sucrose, pH adjusted to 7.6) using a mechanical tissue grinder (OMNI International; see Ref. 6), and total protein concentration was determined by the BCA assay (Pierce) using BSA as the standard. Samples were then solubilized in Laemmli buffer (10 mM Tris, pH 6.8, 1.5% SDS, 6% glycerol, 0.05% bromphenol blue, and 40 mM DTT) and 10 or 20 μg of protein subjected to SDS-PAGE (17) and immunoblotting as described (4). All antibodies were used according to the manufacturer's recommendations. Blots were detected by chemiluminescence (LumiGLO; KPL, Gaithersburg, MD) and visualized by autoradiography.

Immunocytochemistry. Rat kidney blocks containing all kidney zones were dehydrated and embedded in paraffin. The paraffin-embedded tissues were cut into 2-μm sections on a rotary microtome (Micron) and processed for indirect immunoperoxidase labeling as described (9). The sections were dewaxed and rehydrated. Endogenous peroxidase was blocked by 0.5% H_2O_2 in absolute methanol for 30 min at room temperature. To reveal antigens, sections were placed in 1 mM Tris solution (pH 9.0) supplemented with 0.5 mM EGTA and heated to boiling in a microwave oven for 10 min. Nonspecific binding of Ig was prevented by incubating the sections in 50 mM NH_4Cl for 30 min, followed by blocking in PBS supplemented with 1% BSA, 0.05% saponin, and 0.2% gelatin. Sections were incubated overnight at 4°C with primary antibodies diluted in PBS supplemented with 0.1% BSA and 0.3% Triton X-100 and then rinsed with PBS supplemented with 0.1% BSA, 0.05% saponin, and 0.2% gelatin for 3 × 10 min. The sections were washed and then incubated in horseradish peroxidase-conjugated secondary antibody diluted in PBS supplemented with 0.1% BSA and 0.3% Triton X-100. Detection of peroxidase was carried out using diaminobenzidine chromogen (DAKO, Carpinteria, CA).

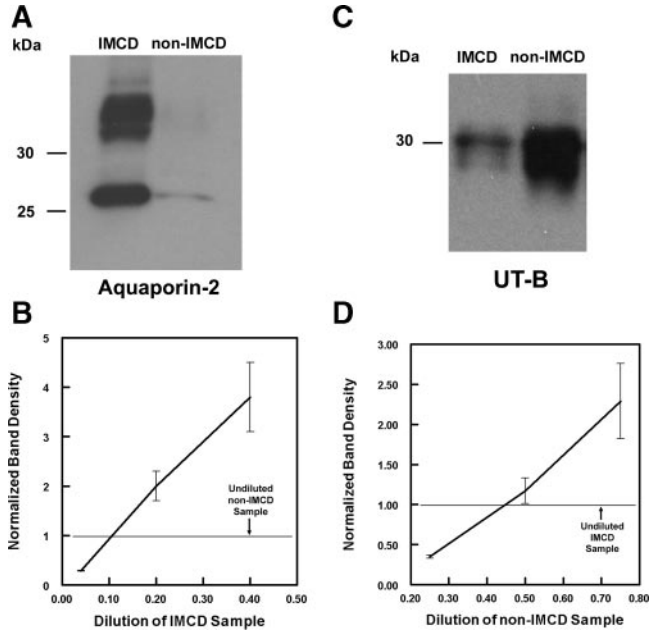

Fig. 1. Confirmation of inner medullary collecting duct (IMCD) enrichment through serial dilution. *A*: immunoblot of aquaporin (AQP)-2 expression in the IMCD vs. non-IMCD fraction; 10 μg protein loaded/lane. Blots were probed with affinity-purified rat AQP2 antibody. *B*: serial dilution of IMCD samples demonstrating a 10-fold enrichment in AQP2 abundance in IMCD. Samples were treated as in *A* and processed for immunoblotting as described ($n = 3$ for each fraction) *C*: immunoblot of urea transporter (UT)-B expression in the IMCD vs. non-IMCD fraction; 20 μg protein/lane. Blots were probed with affinity-purified rat UT-B antibody. *D*: serial dilution of non-IMCD samples demonstrating a 2.3-fold enrichment in UT-B abundance in non-IMCD. Samples were treated as in *C* and processed for immunoblotting as described ($n = 3$ for each fraction).

Statistics. Densitometric analysis of protein immunoblots is expressed as the mean ± SE ($n = 3$) for each group. Unpaired *t*-tests were performed for some experiments to assess the effect of different interventions.

RESULTS

Characterization of IMCD cell purification procedure: enrichment of IMCD cells. We used the vasopressin-sensitive water channel AQP2 (24) as a marker for IMCD cells and the urea transporter UT-B (30) as a representative marker for non-IMCD cells. Because immunoblotting using chemiluminescence on light-sensitive film lacks intrinsic linearity when applied over a wide range, we evaluated the degree of enrichment using serial dilution to determine the degree of dilution needed to equalize band densities between IMCD and non-IMCD fractions. IMCD and non-IMCD fractions were isolated from whole rat inner medulla as described in METHODS. Solubilized proteins were separated by SDS-PAGE, and immunoblots were probed with an antibody to AQP2 (Fig. 1, *A* and *B*). AQP2 was 10.0-fold enriched in the IMCD fraction vs. the non-IMCD fraction [dilution factor in Fig. 1*B*: 0.10 ± 0.07 (SE)]. Samples were also probed with an antibody to UT-B (Fig. 1, *C* and *D*). UT-B was 2.3-fold enriched in the non-IMCD fraction vs. the IMCD fraction [dilution factor in Fig. 1*D*: 0.43 ± 0.11 (SE)]. Based on these values, we can calculate the theoretical maximum and minimum Cy3-to-C5 ratios obtainable using the DIGE technique with these cell fractions (see APPENDIX). The theoretical maximum Cy3-to-C5 ratio obtainable if a given protein is expressed only in IMCD cells is 3.0 (95% confidence interval 2.5–4.3). The theoretical minimum Cy3-to-Cy5 ratio obtainable if a given protein is expressed only in non-IMCD cells is 0.13 (95% confidence interval 0.03–0.22). To conclude that a protein is present in IMCD cells, we take the conservative threshold of two times the upper limit of the 95% confidence interval for the minimum Cy3-to-Cy5 ratio, namely 0.44 (see APPENDIX).

Assessment of experimental variation. Before conducting experiments to compare two different samples by the DIGE technique, we carried out an experiment comparing two nominally identical samples of IMCD homogenate to assess intrinsic experimental variation (Fig. 2). The two samples were from two different rats but were processed identically; thus, the variability seen in this experiment also includes biological variability. Figure 2 shows the distribution of the spot density ratio for all discrete spots detected by the image analysis software and the relation between spot density and log spot density ratio for this experiment. All spot density ratios were between 0.57 and 1.67, whereas the vast majority of spots had density ratios around 1.0. In general, those proteins that showed the largest deviation from unity in this experiment were those with the lowest abundance. As can be appreciated from Fig. 2, the Cy3-to-Cy5 ratio for proteins in the upper 50th percentile of abundance showed a much narrower range of variability. This experiment demonstrates the low level of background variability inherent in two biological samples and also the reproducibility of differential Cy dye labeling.

Identification of proteins present in IMCD cells. To identify major proteins expressed in IMCD cells, rat IMCD and non-IMCD homogenates were prepared and analyzed as described in METHODS. With the DIGE method, each 2-D gel is imaged in three ways, using Cy3 to label IMCD proteins, Cy5 to label non-IMCD proteins, and Sypro Ruby for total protein. Figure

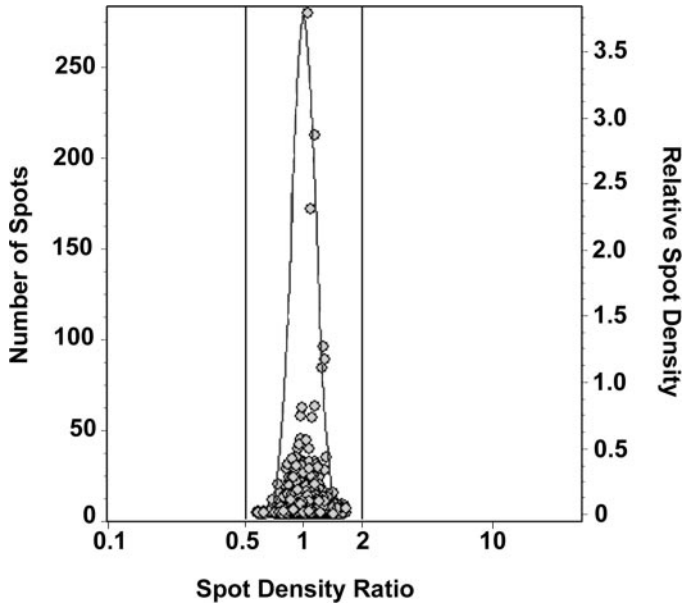

Fig. 2. Assessment of experimental variation. IMCD samples from 2 different rats were labeled with Cy3 or Cy5 dye and analyzed on a single 2-dimensional (2-D) gel. Cy3-to-Cy5 spot density ratio (*x*-axis) is plotted against number of spots (*left y*-axis, curve) and relative density for each spot (*right y*-axis, gray circles).

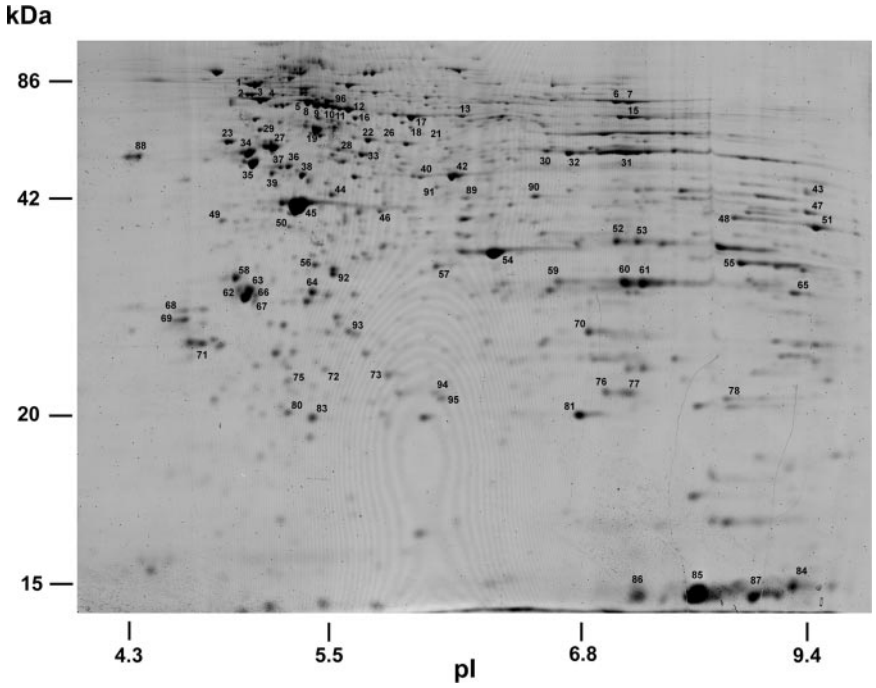

Fig. 3. Sypro Ruby gel image of mixed IMCD and non-IMCD samples. A total of 50 μg of IMCD and 50 μg of non-IMCD cell lysates were mixed and loaded on a single 24-cm immobilized pH gradient (IPG) strip, pH range 3–10. Second-dimension SDS-PAGE was run on a 12.5% polyacrylamide gel. Spots that are numbered correspond to proteins that were correctly identified by matrix-assisted laser desorption ionization-time of flight mass spectrometry (Table 1).

3 shows the 2-D image from Sypro Ruby staining, and Fig. 4 shows selected regions of this gel imaged for either Cy3 (IMCD) or Cy5 (non-IMCD). The spots numbered in Fig. 3 indicate the proteins identified by MALDI-TOF mass spectrometry and are listed in Table 1 with the Cy3-to-Cy5 fluorescence ratios, the theoretical pI values, theoretical molecular weights, and accession numbers of identified proteins. The "expectation" is a likelihood parameter indicating the probability of misidentification of the protein based on mass spectral data alone (see METHODS).

Initially, 85 distinct protein spots were identified (Table 1). In some cases, multiple spots were seen for a given named protein, presumably representing protein modifications. Most of the identified proteins were structural proteins, cytosolic- and membrane-associated enzymes, and signaling intermediates. Of the 85 spots identified, at least 50 appear to be expressed in the IMCD (Cy3/Cy5 $>$ 0.44) according to the criterion established above (see APPENDIX), whereas 10 of these appear to be most highly enriched in IMCD relative to non-IMCD (Cy3/Cy5 $>$ 2). Of the 10 that were highly enriched in IMCD, there were 8 unique identifications as follows: cytokeratins 8 and 18, transglutaminase II, heat shock protein (HSP) 27, aminopeptidase B, T-plastin, HSP70, and lactate dehydrogenase A. Thirty-five spots were identified with Cy3-to-Cy5 ratios $<$0.44, indicating that these proteins could not be identified clearly as being IMCD proteins based on the criterion established above. The lower-molecular-weight form of annexin II and multiple spots of annexin V that were enriched in non-IMCD may reflect differences in posttranslational processing and/or alternative splicing (Fig. 4). Other proteins that were enriched in the non-IMCD fraction included a variety of mitochondrial components as well as Hb-α and -β, presumably from red blood cells in the vasa recta (Fig. 4). The 40 additional identifications at the end of Table 1 represent inner medullary proteins that were identified in preliminary optimization experiments (gels not shown) using only IMCD samples

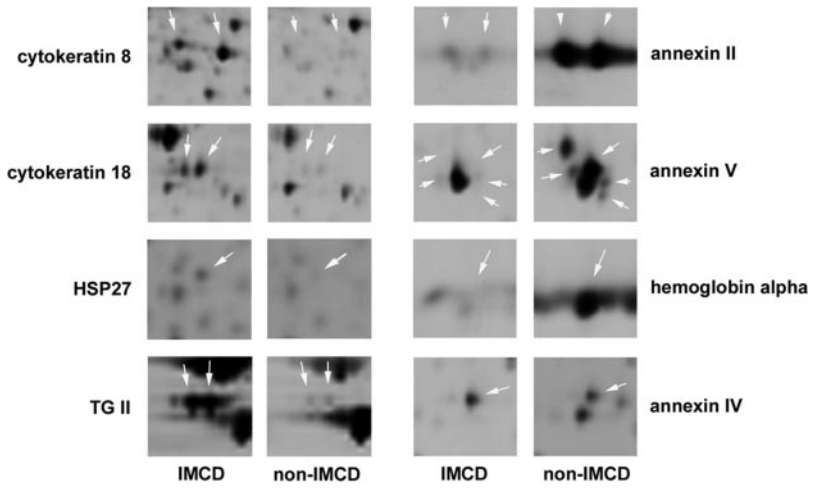

Fig. 4. Comparison of abundances of fluorescently labeled IMCD and non-IMCD proteins. A total of 50 μg of Cy3-labeled (IMCD) and 50 μg of Cy5-labeled (non-IMCD) cell lysates were mixed and loaded on a single 24-cm IPG strip, pH range 3–10. Second-dimension SDS-PAGE was run on a 12.5% polyacrylamide gel. Spots of interest are labeled (arrows). Cytokeratins 8 and 18, heat shock protein (HSP) 27, and transglutaminase II (TG II) increased in IMCD. The lower-molecular-weight form of annexin II, multiple forms of annexin V, and Hb-α were enriched in the non-IMCD fraction. The level of annexin IV was similar between the two samples.

Table 1. *Proteins identified by MALDI-TOF mass spectrometry*

Spot No.	Spot Density Ratio (Cy3/Cy5)*	Protein Identification	pI	Molecular Mass, kDa	*P*	Accession No.
33	6.86	Cytokeratin 8	5.5	52.69	0.000	203734
28	4.69	Cytokeratin 8	5.5	52.69	0.000	203734
2,3	3.27	GTP-binding protein G_h/transglutaminase II	5.0	78.01	0.001	743818
11	3.16	Aminopeptidase B	5.5	70.35	0.002	1754515
10	2.79	T-plastin	5.4	70.80	0.002	2493465
36	2.62	Cytokeratin 18	4.6	45.50	0.020	587518
72	2.46	HSP27	6.1	22.86	0.003	14010865
12	2.41	HSP70	5.6	70.45	0.000	2119721
37	2.06	Cytokeratin 18	4.6	45.50	0.050	587518
55	2.02	Lactate dehydrogenase A	8.7	36.72	0.001	8393706
83	1.95	Phosphatidylethanolamine-binding protein	5.5	20.90	0.001	8393910
93	1.84	Protease 28 α-alpha	5.8	28.73	0.000	8394088
42	1.71	Enolase 1α	6.2	47.44	0.000	6978809
90	1.70	Isocitrate dehydrogenase 1	6.5	47.06	0.000	13928690
21	1.68	Glucose-6-phosphate dehydrogenase	6.2	55.32	0.079	204197
46	1.61	Ca/CaMK1β	6.0	38.65	0.009	8393035
9	1.55	hst70	5.4	69.81	0.001	92355
78	1.55	Peroxiredoxin 1 (HBP23)	8.7	22.32	0.020	6435547
1	1.52	HSP86	4.9	85.20	0.067	14270366
29	1.49	Tubulin-α	4.9	50.91	0.001	223556
73	1.48	Antioxidant protein 2	5.6	24.86	0.001	5902791
71	1.47	Tyrosine 3-/tryptophan 5-monooxygenase activation protein	4.7	27.95	0.002	13487931
54	1.46	Aldehyde reductase 1	6.3	36.24	0.004	6978491
44	1.41	Creatine kinase B	5.3	40.89	0.000	203476
48	1.37	Fructose-bisphosphate aidolase	8.8	39.70	0.083	68186
68	1.34	Tropomyosin 4	4.7	28.55	0.013	6981672
69	1.34	Tyrosine 3-/tryptophan 5-monooxygenase activation protein	4.7	27.95	0.067	13487931
5	1.31	HSP72	5.4	71.14	0.001	347019
49	1.31	Laminin-receptor 1	4.8	32.92	0.022	8393693
27	1.28	Tubulin-α	4.9	50.91	0.001	223556
70	1.25	Carbonic anhydrase 2	6.9	29.27	0.005	9506445
8	1.24	HSP72	5.4	71.14	0.001	347019
34	1.16	Tubulin-β	4.8	50.38	0.000	92930
57	1.15	Malate dehydrogenase-like enzyme	6.2	36.64	0.029	15100179
18	1.14	T-complex 1	5.9	60.86	0.015	6981642
89	1.05	*S*-adenosylhomocystein hydrolase	6.1	47.90	0.023	4139571
15	1.04	Transketolase	7.3	68.37	0.017	1729977
95	1.03	Contraception-associated protein 1	6.3	20.18	0.003	7429594
52	1.02	Annexin II	8.3	39.03	0.000	9247201
75	1.02	NADH-ubiquinone oxidoreductase	6.0	26.85	0.001	128867
80	1.01	Thioredoxin peroxidase 1	5.3	21.94	0.010	8394432
53	0.971	Annexin II	8.3	39.03	0.000	9247201
45	0.952	Actin-β	5.3	42.08	0.003	71620
40	0.935	GDP dissociation inhibitor 2	5.7	51.18	0.013	8393428
76	0.935	Glutathione-*S*-transferase	6.9	23.65	0.006	121749
81	0.926	α-Crystallin, β-chain	6.8	20.07	0.073	117388
77	0.917	Glutathione-*S*-transferase	6.9	23.65	0.006	121749
50	0.855	GTP-binding protein $G\alpha_{i\text{-}2}$	5.3	41.05	0.079	13591955
64	0.694	Annexin IV (ZAP36)	5.3	36.20	0.000	13162351
96	0.568	GRP75	5.9	74.01	0.000	2119726
94	0.420	Peroxiredoxin 3	7.2	28.59	0.023	11968132
39	0.369	Protein disulfide isomerase A6	4.9	47.60	0.001	2501206
13	0.356	Succinate-ubiquinone reductase	6.8	72.62	0.064	16117830
88	0.339	Calreticulin	4.3	48.15	0.006	11693172
19	0.339	HSP60	5.3	58.08	0.014	1334284
22	0.330	Protein disulfide isomerase A3	5.9	57.06	0.000	1352384
31	0.329	F1 ATPase A	8.4	55.38	0.000	6729934
16	0.321	Dihydrolipoamide acetyltransferase	5.7	59.15	0.020	266685
56	0.321	Pyruvate dehydrogenase E1-β	5.9	39.34	0.006	1352624
26	0.315	Protein disulfide isomerase A3	5.9	57.06	0.000	1352384
6	0.309	Mitochondrial aconitase	8.2	86.20	0.000	13242312
7	0.308	Mitochondrial aconitase	8.2	86.20	0.000	13242312
4	0.300	Protein disulfide isomerase A4 (ERP72)	5.0	73.13	0.085	729436
23	0.290	Iodothyronine 5′-monodeiodinase	4.9	54.39	0.002	202549
38	0.269	Ribonucleoprotein F	5.3	46.05	0.012	4153896
65	0.262	Voltage-dependent anion channel-1	8.5	32.67	0.000	10720216

Table 1. *Continued*

Spot No.	Spot Density Ratio (Cy3/Cy5)*	Protein Identification	pI	Molecular Mass, kDa	*P*	Accession No.
32	0.256	Glutamate dehydrogenase	8.3	61.75	0.000	118543
30	0.245	Long-chain fatty acid CoA ligase 5	7.1	77.24	0.060	6016484
51	0.238	Glutamate oxaloacetate transaminase 2	9.4	47.70	0.002	6980972
35	0.236	F1 ATPase B	4.9	51.33	0.000	6729935
17	0.220	Albumin	6.1	70.70	0.000	113580
91	0.216	Phenol sulfotransferase	6.1	35.86	0.028	13929030
47	0.206	Ubiquinol-cytochrome *c* reductase complex core protein 2	9.2	48.41	0.002	418146
67	0.126	Annexin V	5.0	33.95	0.000	1421099
62	0.116	Annexin V	5.0	33.95	0.000	1421099
43	0.112	HSP47	9.0	46.61	0.043	8393057
66	0.107	Annexin V	5.0	33.95	0.000	1421099
87	0.072	Hemoglobin-α	8.7	15.44	0.006	1304381
86	0.067	Hemoglobin-β	8.2	15.93	0.090	546056
84	0.066	Hemoglobin-β, minor form	9.2	16.08	0.047	122529
63	0.065	Annexin V	5.0	33.95	0.000	1421099
60	0.056	Annexin II	8.3	39.03	0.028	9247201
85	0.050	Hemoglobin-α	7.9	15.48	0.007	1304381
61	0.043	Annexin II	8.3	39.03	0.083	9247201
58	0.023	Annexin V	5.0	33.95	0.000	1421099
	†	26S protease regulatory subunit 6A	5.1	49.43	0.026	2492523
	†	26S protease regulatory subunit 6B	5.1	47.50	0.031	2492517
	†	Adenine phosphoribosyltransferase	6.2	19.76	0.000	543829
	†	Adenylyl cyclase-associated protein homolog MCH1	7.2	51.91	0.005	539940
	†	Aldehyde dehydrogenase family 9, subfamily A1	6.6	54.55	0.000	11560095
	†	α-II spectrin	5.2	285.38	0.000	1495198
	†	α-Actinin 4	5.2	105.22	0.012	13123941
	†	Annexin I	7.0	39.14	0.000	235879
	†	Calpain small subunit	5.3	28.18	0.008	1794205
	†	Carboxylesterase	6.1	62.41	0.060	57554
	†	Cartilage proteoglycan protein	4.7	41.07	0.005	92062
	†	Clatherin heavy polypeptide	5.5	193.29	0.000	9506497
	†	c-*met*/Hepatocyte growth factor receptor	8.2	15.34	0.005	2443209
	†	Collagen XVIII	9.8	25.56	0.074	6007583
	†	Damage-specific DNA-binding protein 1	5.2	128.52	0.004	9843869
	†	Dihydropyrimidinase-related protein-2	6.0	62.66	0.000	1351260
	†	Glutaminase	8.5	74.88	0.000	92297
	†	Glyceraldehyde-3-phosphate dehydrogenase	8.4	36.10	0.029	8393418
	†	Guanine nucleotide-binding protein-β_1	5.5	38.17	0.000	13591874
	†	Ischemia-responsive 94-kDa protein	5.1	94.84	0.039	6651427
	†	Lactate dehydrogenase B	5.7	36.88	0.002	6981146
	†	Lamin A	6.2	71.91	0.002	453180
	†	Lamin B1	5.2	66.82	0.000	1575794
	†	Major vault protein	5.6	99.00	0.005	2498602
	†	Mitochondrial trifunctional enzyme-α	9.4	83.24	0.000	2494234
	†	Phosphoglycerate mutase B chain	6.7	28.93	0.000	112128
	†	PKA type I regulatory subunit	5.3	43.31	0.043	6981396
	†	Prolactin receptor	5.2	36.78	0.060	112201
	†	Propionyl-CoA carboxylase-α	6.3	78.22	0.001	92654
	†	Protease 28 subunit-β	5.5	27.07	0.026	8394091
	†	Proteasome 26S subunit ATPase	5.6	48.96	0.001	15100181
	†	Proteasome subunit-α type 3	5.3	28.63	0.003	8394066
	†	Proteasome subunit-α type 5	4.8	26.54	0.004	8394072
	†	Proteasome subunit-α type 6	6.3	27.84	0.099	8394076
	†	Proteasome z subunit	8.6	30.25	0.003	9719458
	†	Protein phosphatase 2	5.3	36.16	0.000	8394018
	†	Senescence marker protein-30	5.4	33.94	0.019	2507128
	†	Transitional ER ATPase	5.1	90.02	0.000	1174637
	†	Translation elongation factor 1-α_2	9.3	50.47	0.010	15805031
	†	Translation elongation factor 2	6.4	96.24	0.000	8393296

Data for isoelectric point (pI) and molecular mass are theoretical values. The probability (*P*) of misidentification is based on peptide mass fingerprint alone. *Inner medullary collecting duct (IMCD) vs. non-IMCD. †Identified in isolated IMCD cells in initial optimization experiments for sample loading and detergent solubilization (CHAPS, ASB-16). MALDI-TOF, matrix-assisted laser desorption ionization-time of flight.

and were not directly compared with a corresponding non-IMCD sample.

Figure 5*A* shows a typical MALDI-TOF peptide mass spectrum for one of the proteins that was found to be preferentially expressed in the IMCD fraction. Corresponding amino acid residue numbers are indicated on peaks that were matched to the identified protein based on a query of the nonredundant database ProFound. The top four candidate proteins, including attributes such as pI, molecular weight, and expectation, are also listed (Fig. 5*B*). The protein identified was T-plastin, with an expectation value of 0.002 (0.2% chance of an incorrect identification) and coverage of 21.5 (21.5% of the total protein length included in the identified peptide masses). For all identifications reported in Table 1, confirmation was established by comparing the theoretical pI and molecular weight of the identified protein with the coordinates of the original spot on the gel.

Confirmation of protein identifications by immunoblotting. Selected proteins identified by mass spectrometry were confirmed by immunoblotting. Cytokeratins 8 and 18 (Fig. 6, *A* and *B*), HSP27 (Fig. 6, *C* and *D*), and transglutaminase II (6, *E* and *F*) were all enriched in IMCD samples, supporting the results obtained using DIGE. The lower-molecular-weight form of annexin II was enriched in non-IMCD fractions (Fig. 6, *G* and *H*), a result that was also predicted by the analysis of the Cy3 and Cy5 images. Annexin IV, aldehyde reductase I, carbonic anhydrase II, and β-actin, which were evenly distributed between the two fractions based on 2-D gel analysis, were present at similar levels in both fractions on the immunoblot (Fig. 6, *I–P*). These observations demonstrate the validity of the DIGE technique applied to the analysis of IMCD proteins.

Localization of selected proteins by immunocytochemistry. Paraffin-embedded sections of rat kidney were processed for immunocytochemistry as described (9). AQP2 was employed as an IMCD-specific marker (Fig. 7*A*). Sections stained for cytokeratin 8/18, HSP27, and transglutaminase II showed predominant staining in IMCD (Fig. 7, *B–D*), consistent with the DIGE results. Annexin II labeling was present in IMCD (Fig. 7*E*) but was intense in thin limb segments as well. Annexin IV was present in both IMCD and non-IMCD cells, with slightly greater labeling found in IMCD (Fig. 7*F*). These results support the inferred tissue distribution obtained through 2-D gel analysis and immunoblotting of IMCD and non-IMCD fractions.

DISCUSSION

In this study, we describe a standardized approach for isolation of native renal IMCD cells from rat kidney, which we propose as a beginning point for studies aimed at definition of the IMCD proteome. Although IMCD cells constitute a major component of the inner medulla, making up ~30% of the volume of the inner medulla (16), other cell types are present and contribute a substantial fraction of inner medullary proteins. Hence, for proteomic analysis of the IMCD cells, it is inadequate to analyze whole inner medullas. The IMCD cell purification procedure, modified from the work of Stokes et al. (29), provides an easily implemented means of isolating large numbers of IMCD cells from rat inner medulla. Preliminary immunoblotting documented that there was a 10-fold enrichment of a previously identified collecting duct marker protein, AQP2. Here, we used DIGE (31) to further characterize the approach and to identify relatively abundant proteins expressed in the IMCD.

DIGE is a method that is based on attachment of different fluorescent dyes to two populations of proteins for quantification of protein abundance ratios. We used DIGE to compare the IMCD fraction with the non-IMCD elements of the inner medulla. Overall, we identified 50 proteins expressed in the IMCD, of which 10 were shown to be enriched in the IMCD fraction twofold or more (Table 1). An additional 35 proteins were found to be predominantly expressed in the non-IMCD fraction (Cy3-to-Cy5 ratio <0.44). The 50 proteins found in the IMCD in this study add to the 378 proteins identified in the

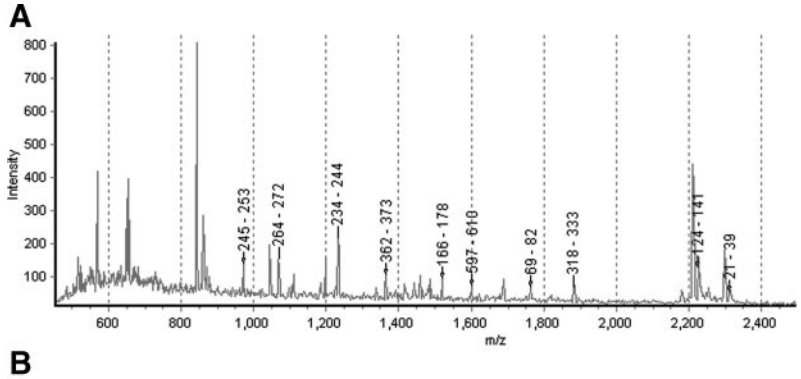

Fig. 5. Protein identification by mass spectrometry. *A*: peptide mass fingerprint for trypsin digest of *spot 10*. The *x*-axis represents mass-to-charge ratio (m/z), whereas the *y*-axis represents relative abundance. Labels correspond to amino acid numbers of each peptide fragment. *B*: after searching the ProFound database, the software identified T-plastin as the top candidate with an expectation value of 0.002 and a coverage of 21.5%.

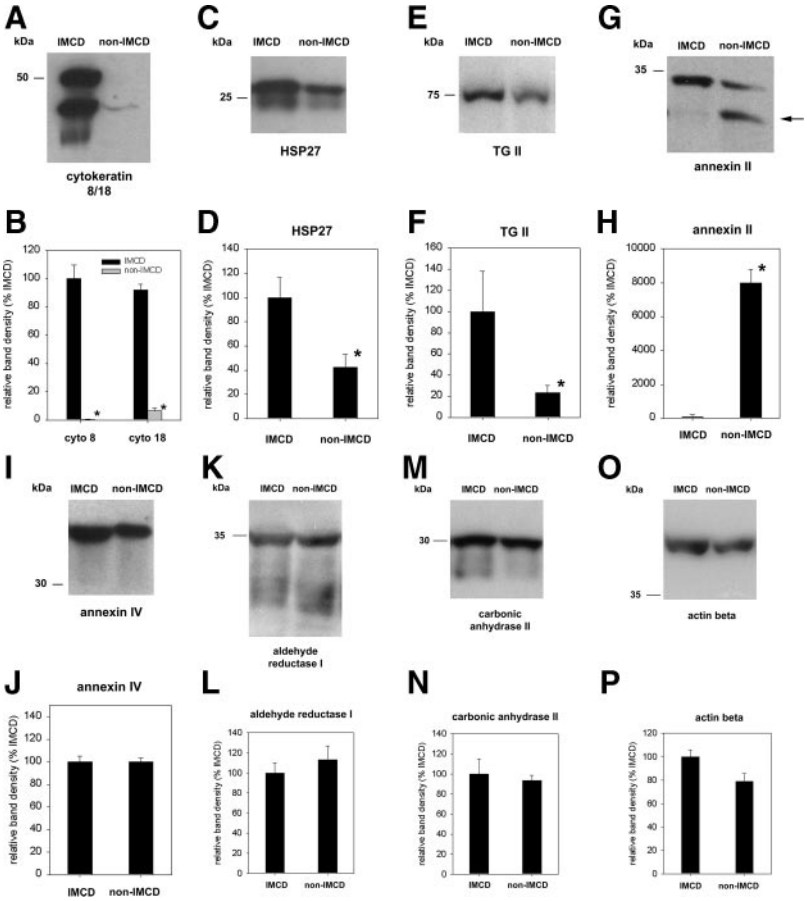

Fig. 6. Validation of identified proteins by immunoblotting. IMCD and non-IMCD (20 μg) cell lysates were analyzed by immunoblotting and probed using antibodies against cytokeratin (cyto) 8/18 (*A* and *B*), HSP27 (*C* and *D*), TG II (*E* and *F*), annexin II (*G* and *H*), annexin IV (*I* and *J*), aldehyde reductase I (*K* and *L*), carbonic anhydrase II (*M* and *N*), and β-actin (*O* and *P*). Arrow indicates the lower-molecular-weight form of annexin II. For quantitation of band densities, samples were prepared for immunoblotting as described in METHODS ($n = 3$ for each fraction; $^*P < 0.05$) and represented as %IMCD expression for each protein.

literature to be expressed in the collecting duct (18; URL: http://mrb.niddk.nih.gov/cddb), although undoubtedly many lower-abundance IMCD proteins remain to be identified. We detected a wide variety of proteins, from cytoskeletal proteins and associated factors such as cytokeratins 8 and 18, β-actin, α- and β-tubulin, α-actinin, T-plastin, tropomyosin, α-II spectrin, and clathrin to regulatory factors such as GTP-binding proteins G_h and $G\alpha_{i\text{-}2}$, GDP dissociation inhibitor 2, CaMK 1, PKA type I regulatory subunit, and annexins I, II, IV, and V. In addition, we were able to detect differential expression profiles for a number of proteins in a comparison between IMCD and non-IMCD pools from rat inner medulla, including differences in the spot pattern for both annexin II and annexin V that may reflect alternative splice variants or changes in posttranslational processing. Immunoblotting and immunohistochemistry confirmed the relative expression level and distribution of selected proteins identified by 2-D gel analysis.

The IMCD cell is a relatively simple cell from a functional point of view. IMCD cell functions can be classified into the following two general categories: *1*) regulated transport, which determines the final composition of urine, and *2*) maintenance of IMCD cell form, integrity, and number. Several of the proteins found to be enriched in the IMCD may play potentially important roles in these two functions of the IMCD. Because other inner medullary cells would be subjected to the same environmental challenges as IMCD cells, it seems likely that many of the proteins enriched in IMCD cells over non-IMCD cells may be devoted to the former general function, i.e., regulation of transport.

There were 10 proteins that were highly enriched in the IMCD fraction (Cy3/Cy5 >2.0). [Note: Calculations based on *Eq. 1* in the APPENDIX indicate that a Cy3-to-Cy5 ratio of 2 corresponds to an abundance ratio (A_{IMCD}/A_{non}) of 4.] These proteins included cytokeratins 8 and 18, which are the major intermediate filament proteins expressed in collecting duct epithelium (10) and hence play an important role in determining cell structure. Also highly expressed in the IMCD cells was transglutaminase II, also known as G protein G_h, which is a unique nonheterotrimeric GTP-binding protein, distinct from the small GTP-binding proteins (11). In addition to its putative role in signal transduction through adrenergic receptors and its ability to activate the phospholipase C-δ1 pathway in various cell types, it also possesses a distinct cross-linking function by catalyzing the formation of ε-(γ-glutamyl)lysine isopeptide bonds (11, 23). Extensive evidence points to an important role for transglutaminase II in vesicular trafficking (3, 19), leading us to hypothesize that it could be an element in processes responsible for vasopressin-induced AQP2 trafficking in the IMCD. Also enriched in IMCD was the heat shock protein HSP27, which exhibits an expression pattern that parallels the corticomedullary osmotic gradient (20) and may play a role in the adaptive response of the inner medulla to fluctuations in extracellular osmolality (1, 22). Aminopeptidase B is a Zn^{2+}-metallo-exopeptidase that cleaves the amino-terminal argininyl

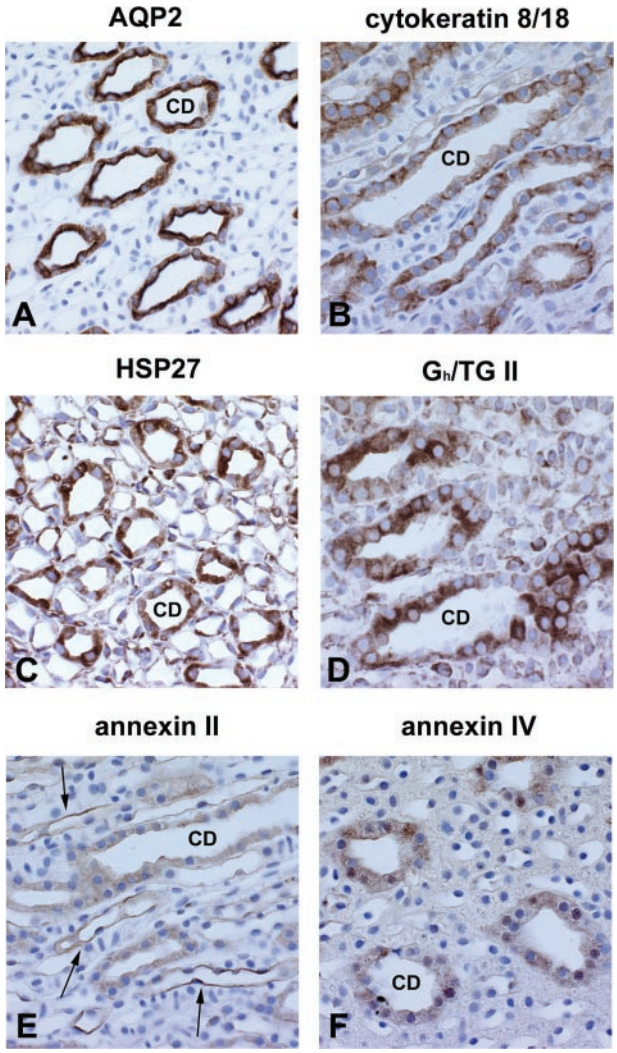

Fig. 7. Localization of proteins by immunohistochemistry. Sections of rat inner medulla were probed using antibodies against AQP2 (*A*), cytokeratin 8/18 (*B*), HSP27 (*C*), transglutaminase II (*D*), annexin II (*E*), and annexin IV (*F*). A representative IMCD (CD) is labeled in each image. In *E*, labeled thin limb segments are indicated by arrows.

or lysyl residue from peptides. For example, it acts on ANG III, converting it to ANG IV (27), a potential mediator of both renal and cerebral control of salt balance (8, 32).

Although the DIGE technique is a relatively efficient and reliable method for proteomics studies, two potential drawbacks remain that plague nearly every system that relies on 2-D electrophoresis. The first is the difficulty in detecting hydrophobic proteins, particularly those with multiple transmembrane domains. Although the use of both thiourea and more powerful solubilizing agents such as the sulfobetaine detergents amidosulfobetaine-14 and -16 have yielded positive results (21), integral membrane proteins have remained extremely difficult to separate by conventional 2-D electrophoresis. Using our solubilization protocol of 2 M thiourea, 7 M urea, and 4% CHAPS, we were able to detect only two transmembrane proteins [the prolactin receptor, which has a single transmembrane domain (13), and voltage-dependent anion channel-1, which is present in the outer mitochondrial membrane (5)]. Further experimentation with other detergents may reveal additional integral membrane proteins. The second disadvantage of 2-D-based systems is the strong bias toward high-abundance proteins (15). This is especially important when considering that many important signaling factors are of low abundance and may not show up when the gel is imaged. Furthermore, ion channel proteins such as the ENaC subunits tend to be expressed in cells at relatively low levels and are difficult to detect with this method. This problem is potentially addressable through subcellular fractionation techniques that can enrich proteins present in specific organelles (12). In addition, high-density antibody microarrays may provide a complementary tool for detecting low-abundance signaling intermediates and transcription factors that are not dectectable by 2-D electrophoresis (28).

Despite these limitations, we have demonstrated the feasibility of large-scale identification of proteins in a single renal cell type, the IMCD cell, a necessary first step in application of complex systems modeling techniques to the understanding of protein networks involved in regulation of solute and water excretion. The DIGE technique may prove useful for studying collecting duct regulation in both normal and disease states such as vasopressin escape, renal hypertension, and nephrogenic diabetes insipidus.

APPENDIX 1

The theoretical Cy3-to-Cy5 ratio (R) for these DIGE experiments can be calculated as

$$R = \frac{A_{IMCD} f_1 + A_{non\text{-}IMCD}(1 - f_1)}{A_{IMCD} f_2 + A_{non\text{-}IMCD}(1 - f_2)}$$

where, A_{IMCD} is the abundance of a given protein in IMCD cells (mg/mg total protein); $A_{non\text{-}IMCD}$ is the abundance of a given protein in non-IMCD cells (mg/mg total protein); f_1 is the fraction of total protein in *fraction 1* that is from IMCD cells; and f_2 is the fraction of total protein in *fraction 2* that is from IMCD cells. (This equation assumes that the Cy3 and Cy5 fluorescence for any given protein spot is linearly related to the amount of labeled protein.) If *fraction 1* is taken as the "IMCD-enriched fraction," f_1 can be evaluated as $10/(10 + 1) = 0.909$, based on the value of the enrichment for AQP2 (10.0) in the IMCD-enriched fraction. If *fraction 2* is taken as the "non-IMCD-enriched fraction," f_2 can be evaluated as $1/(2.3 + 1) = 0.303$, based on the value of the enrichment for UT-B (2.3) in the IMCD-enriched fraction. Using these values, we can calculate that, for a protein expressed only in IMCD ($A_{non\text{-}IMCD} = 0$), $R = 3.0$, i.e., $R_{max} = 3.0$. Furthermore, for a protein only expressed in non-IMCD cells ($A_{IMCD} = 0$), $R = 0.13$, i.e., $R_{min} = 0.13$. Based on the statistical uncertainty in our estimates of the enrichment values for AQP2 and UT-B, the 95% confidence interval for R_{min} can be calculated to be 0.03–0.22. The latter value forms the basis of our definition of minimum Cy3-to-Cy5 ratio criterion to conclude that a given protein is expressed in IMCD cells. Based on this, we adopt the conservative criterion that R must be at least two times the upper bound of the 95% confidence interval for R_{min}, i.e., $R > 0.44$, to conclude that a particular protein is expressed in IMCD cells.

GRANTS

This study was funded by the Intramural Budget of the National Heart, Lung, and Blood Institute (National Institutes of Health, project no. Z01-HL-01282-KE to M. A. Knepper). Support for B. W. M. van Balkom was provided by the Nephrogenic Diabetes Insipidus Foundation, the American Heart Association, the Dutch Organization for Scientific Research and De Drie Lichten Foundation.

REFERENCES

1. **Beck FX, Burger-Kentischer A, and Muller E.** Cellular response to osmotic stress in the renal medulla. *Pflügers Arch* 436: 814–827, 1998.
2. **Chou CL, DiGiovanni SR, Luther A, Lolait SJ, and Knepper MA.** Oxytocin as an antidiuretic hormone. II. Role of V2 vasopressin receptor. *Am J Physiol Renal Fluid Electrolyte Physiol* 269: F78–F85, 1995.
3. **Davies PJ, Davies DR, Levitzki A, Maxfield FR, Milhaud P, Willingham MC, and Pastan IH.** Transglutaminase is essential in receptor-mediated endocytosis of alpha 2-macroglobulin and polypeptide hormones. *Nature* 283: 162–167, 1980.
4. **Davis JQ and Bennett V.** Brain ankyrin. A membrane-associated protein with binding sites for spectrin, tubulin, and the cytoplasmic domain of the erythrocyte anion channel. *J Biol Chem* 259: 13550–13559, 1984.
5. **De Pinto VD and Palmieri F.** Transmembrane arrangement of mitochondrial porin or voltage-dependent anion channel (VDAC). *J Bioenerg Biomembr* 24: 21–26, 1992.
6. **Ecelbarger CA, Nielsen S, Olson BR, Murase T, Baker EA, Knepper MA, and Verbalis JG.** Role of renal aquaporins in escape from vasopressin-induced antidiuresis in rat. *J Clin Invest* 99: 1852–1863, 1997.
7. **Garty H and Palmer LG.** Epithelial sodium channels: function, structure, and regulation. *Physiol Rev* 77: 359–396, 1997.
8. **Grove KL and Deschepper CF.** High salt intake differentially regulates kidney angiotensin IV AT4 receptors in Wistar-Kyoto and spontaneously hypertensive rats. *Life Sci* 64: 1811–1818, 1999.
9. **Hager H, Kwon TH, Vinnikova AK, Masilamani S, Brooks HL, Frokiaer J, Knepper MA, and Nielsen S.** Immunocytochemical and immunoelectron microscopic localization of α-, β-, and γ-ENaC in rat kidney. *Am J Physiol Renal Physiol* 280: F1093–F1106, 2001.
10. **Hemmi A and Mori Y.** Immunohistochemical study of cytokeratin distribution in the collecting duct of the human kidney. *Acta Pathol Jpn* 41: 516–520, 1991.
11. **Im MJ, Russell MA, and Feng JF.** Transglutaminase II: a new class of GTP-binding protein with new biological functions. *Cell Signal* 9: 477–482, 1997.
12. **Kernec F, Unlu M, Labeikovsky W, Minden JS, and Koretsky AP.** Changes in the mitochondrial proteome from mouse hearts deficient in creatine kinase. *Physiol Genomics* 6: 117–128, 2001.
13. **Kline JB and Clevenger CV.** Identification and characterization of the prolactin-binding protein in human serum and milk. *J Biol Chem* 276: 24760–24766, 2001.
14. **Knepper M and Burg M.** Organization of nephron function. *Am J Physiol Renal Fluid Electrolyte Physiol* 244: F579–F589, 1983.
15. **Knepper MA.** Proteomics and the kidney. *J Am Soc Nephrol* 13: 1398–1408, 2002.
16. **Knepper MA, Danielson RA, Saidel GM, and Post RS.** Quantitative analysis of renal medullary anatomy in rats and rabbits. *Kidney Int* 12: 313–323, 1977.
17. **Laemmli UK.** Cleavage of structural proteins during the assembly of the head of bacteriophage T4. *Nature* 227: 680–685, 1970.
18. **Legato J, Knepper MA, Star RA, and Mejia R.** Database for renal collecting duct regulatory and transporter proteins. *Physiol Genomics* 13: 179–181, 2003.
19. **Levitzki A, Willingham M, and Pastan I.** Evidence for participation of transglutaminase in receptor-mediated endocytosis. *Proc Natl Acad Sci USA* 77: 2706–2710, 1980.
20. **Medina R, Cantley L, Spokes K, and Epstein FH.** Effect of water diuresis and water restriction on expression of HSPs- 27, -60 and -70 in rat kidney. *Kidney Int* 50: 1191–1194, 1996.
21. **Molloy MP.** Two-dimensional electrophoresis of membrane proteins using immobilized pH gradients. *Anal Biochem* 280: 1–10, 2000.
22. **Muller E, Neuhofer W, Burger-Kentischer A, Ohno A, Thurau K, and Beck F.** Effects of long-term changes in medullary osmolality on heat shock proteins HSp25, HSP60, HSP72 and HSP73 in the rat kidney. *Pflügers Arch* 435: 705–712, 1998.
23. **Murthy SN, Lomasney JW, Mak EC, and Lorand L.** Interactions of G_h/transglutaminase with phospholipase Cδ1 and with GTP. *Proc Natl Acad Sci USA* 96: 11815–11819, 1999.
24. **Nielsen S, DiGiovanni SR, Christensen EI, Knepper MA, and Harris HW.** Cellular and subcellular immunolocalization of vasopressin-regulated water channel in rat kidney. *Proc Natl Acad Sci USA* 90: 11663–11667, 1993.
25. **Nielsen S, Frokiaer J, Marples D, Kwon TH, Agre P, and Knepper MA.** Aquaporins in the kidney: from molecules to medicine. *Physiol Rev* 82: 205–244, 2002.
26. **Peng J and Gygi SP.** Proteomics: the move to mixtures. *J Mass Spectrom* 36: 1083–1091, 2001.
27. **Prieto I, Arechaga G, Segarra AB, Alba F, de Gasparo M, and Ramirez M.** Effects of dehydration on renal aminopeptidase activities in adult male and female rats. *Regul Pept* 106: 27–32, 2002.
28. **Schweitzer B and Kingsmore SF.** Measuring proteins on microarrays. *Curr Opin Biotechnol* 13: 14–19, 2002.
29. **Stokes JB, Grupp C, and Kinne RK.** Purification of rat papillary collecting duct cells: functional and metabolic assessment. *Am J Physiol Renal Fluid Electrolyte Physiol* 253: F251–F262, 1987.
30. **Timmer RT, Klein JD, Bagnasco SM, Doran JJ, Verlander JW, Gunn RB, and Sands JM.** Localization of the urea transporter UT-B protein in human and rat erythrocytes and tissues. *Am J Physiol Cell Physiol* 281: C1318–C1325, 2001.
31. **Unlu M, Morgan ME, and Minden JS.** Difference gel electrophoresis: a single gel method for detecting changes in protein extracts. *Electrophoresis* 18: 2071–2077, 1997.
32. **Wright JW and Harding JW.** Important role for angiotensin III and IV in the brain renin-angiotensin system. *Brain Res Rev* 25: 96–124, 1997.
33. **Yan JX, Devenish AT, Wait R, Stone T, Lewis S, and Fowler S.** Fluorescence two-dimensional difference gel electrophoresis and mass spectrometry based proteomic analysis of *Escherichia coli*. *Proteomics* 2: 1682–1698, 2002.
34. **Zhang W and Chait BT.** ProFound: an expert system for protein identification using mass spectrometric peptide mapping information. *Anal Chem* 72: 2482–2489, 2000.
35. **Zhou G, Li H, DeCamp D, Chen S, Shu H, Gong Y, Flaig M, Gillespie JW, Hu N, Taylor PR, Emmert-Buck MR, Liotta LA, Petricoin EF, III, and Zhao Y.** 2D differential in-gel electrophoresis for the identification of esophageal scans cell cancer-specific protein markers. *Mol Cell Proteomics* 1: 117–124, 2002.